Sixth International Symposium on Turbulence and Shear Flow Phenomena
Seoul, Korea, 22-24 June 2009

SPATIO-TEMPORALLY PERIODIC CONTROL FOR TURBULENT FRICTION DRAG REDUCTION

Aiko YAKENO, Yosuke HASEGAWA and Nobuhide KASAGI
Department of Mechanical Engineering
The University of Tokyo
Hongo 7-3-1, Bunkyo-ku, Tokyo 113-8656, Japan
yakeno@thtlab.t.u-tokyo.ac.jp

ABSTRACT

We evaluate the pre-determined control with temporally- and spatially-periodic spanwise velocity inputs at the wall in a fully developed two-dimensional turbulent channel flow. The spatially-periodic control generally achieves better performance than the temporally-periodic control, the latter of which is called conventionally the spanwise wall-oscillation control. To analyze the drag reducing mechanisms, we focus on the near-wall structures such as quasi-streamwise vortices and low-speed streaks. As a result, it is found that the drag is reduced through the modified spatial phase-relationship between the streamwise vortex and the low-speed streak.

INTRODUCTION

Background and Objectives

Turbulence control should have a substantial impact on reduction of energy consumption and mitigating environmental impacts. For example, the turbulent friction drag accounts for about a half of total energy consumed by an aircraft (Filippone, 2000), so that various control schemes have been proposed and tested.

Compared with passive control, active control has a higher potential to manipulate turbulent flows more flexibly and robustly. Among active control schemes, predetermined control recently attracts much attention because it does not need numerous arrayed miniature sensors and actuators, which are to be distributed over a surface for feedback control. Recently, some spatio-temporally predetermined controls have been proposed, e.g., spanwise wall-oscillation control (Jung *et al*., 1992), local temporally-periodic blowing (Tardu, 1998), spanwise/streamwise traveling wave control (Du and Karniadakis, 2000; Min *et al*., 2006). Among them, control inputs are generally known to be more effective when applied in the spanwise direction than in other directions. However, the detailed drag reduction mechanism has not been fully understood.

A general expression of these spanwise control inputs is given by:

$$w_{wall}(x,z,t) = W_0 \cdot \mathrm{Real}\left[\exp\left\{i\left(\omega t + k_x x + k_z z\right)\right\}\right], \qquad (1)$$

where $\omega = 2\pi/T$, $k_x = 2\pi/\lambda_x$ and $k_z = 2\pi/\lambda_z$. Note that T, λ_x and λ_z are the time period and wavelengths in the streamwise and spanwise direction, respectively. Obviously, when $\omega \neq 0$ and $k_x = k_z = 0$, Eq. (1) corresponds to the conventional wall-oscillation control. In this paper, we refer to it as the temporally-periodic control.

The above-mentioned predetermined controls commonly suffer from large power input, although they generally achieve considerable drag reduction. The temporally-periodic control achieves a drag reduction of over 45%, while the highest energy saving rate is 7% at the most when the oscillation period is $T^+ = 125$ and the amplitude is $W_0^+ = 4.5$ (Quadrio and Ricco, 2004). Here, the variable with a superscript of + represents a value in the wall units. Hence, one of major issues is to develop a new control scheme that brings large drag reduction rate with less power input. Recently, a new control input, which is stationary, but longitudinally-periodic, has been proposed, and it is found more effective in terms of the net energy saving than the conventional temporally-periodic control. This control input corresponds to the case when $k_x \neq 0$ and $\omega = k_z = 0$ in Eq. (1) (as shown in Fig. 1), and is named a spatially-periodic control.

In this paper, we try to assess the temporally- and spatially-periodic controls. By systematically changing the temporal period and the wavelength of the control input, we evaluate the two control schemes in terms of the net energy saving, and discuss the optimal periodicity in the two controls. Finally, we discuss the drag reduction mechanisms by investigating the near-wall coherent structures.

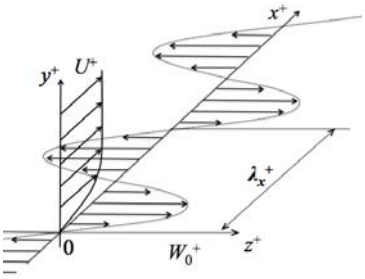

Fig. 1 Schematic of spatially-periodic input at the wall.

Performance Indices for Control

We consider a fully developed turbulent channel flow driven by a pressure gradient under a constant mass flow rate condition. The pumping power P is defined with the channel half-width δ as:

$$P = \int_0^{2\delta} \left(-\overline{u}(y)\frac{\partial \overline{p}}{\partial x}\right) dy. \qquad (2)$$

The instantaneous power input for the spanwise wall motion w_{wall} is given by:

$$P_{in} = \frac{1}{T_\infty}\int_{T_\infty}\left\{\frac{1}{L_x}\frac{1}{L_z}\int_{L_x}\int_{L_z}\left(w_{wall}\left.\frac{\partial w}{\partial y}\right|_{y=0}\right)dxdz\right\}dt, \quad (3)$$

where L_x and L_z are the streamwise and spanwise lengths of the computational domain, respectively, and y is the distance from the wall. In order to evaluate a control scheme, we focus on the following three quantities, i.e., drag reduction rate, gain and energy saving rate.

Drag Reduction Rate: the ratio of the friction drag coefficient C_f to that in the uncontrolled flow:

$$DR = \left(C_{f0} - C_f\right)/C_{f0}. \quad (4)$$

A variable with a subscript of 0 represents a quantity in the uncontrolled case.

Gain: the reduction of flow pumping power input divided by the control power input.

$$G = \left(P_0 - P\right)/P_{in}. \quad (5)$$

Energy Saving Rate: the reduction of total power consumption divided by the pumping power in the uncontrolled flow.

$$S = \left(P_0 - P - P_{in}\right)/P_0. \quad (6)$$

COMPUTATIONAL METHODS

Governing equations are the incompressible Navier-Stokes and continuity equations. We use a periodic boundary condition in the streamwise and spanwise directions, and a no-slip condition at the two walls. A central finite-difference method is adopted for spatial discretization with the second-order of accuracy. The second order Adams-Bashforth method is used for convection terms, while the Crank-Nicolson method for viscous terms. A fractional step method is applied to decouple pressure from the Navier-Stokes equation.

All simulations are performed under a constant streamwise flow rate U_b unless otherwise stated. The bulk Reynolds number based on U_b and the channel half-width δ is $Re_b = 2228$, which corresponds to the friction Reynolds number $Re_\tau = 150$ in the uncontrolled case. The computational domain is $2.5\pi\delta \times 2\delta \times \pi\delta$, in the streamwise, wall-normal and spanwise directions, respectively. The number of grids is $(N_x, N_y, N_z) = (64, 128, 64)$, while the spatial resolutions are $\Delta x^+ = 18.4$, $\Delta y^+ = 0.189 \sim 5.70$ and $\Delta z^+ = 7.36$. In the case of spatially-periodic control, the streamwise domain is extended in accordance with the streamwise wavelength of the control input ($L_x = 2.5\pi\delta \sim 4\pi\delta$, $\Delta x^+ = 9.20 \sim 18.4$). As for the control input, parameters in the temporally-periodic control are the amplitude W_0^+ and the oscillation period T^+, while W_0^+ and the streamwise wavelength λ_x^+ in spatially-periodic control. By systematically changing the above two parameters, 256 computations are repeated for each control scheme.

CONTROL EFFECT

Figures 2 (a) and (b) show obtained drag reduction rate in temporally- and spatially-periodic controls. In both figures, the vertical axis is the amplitude W_0^+, while the horizontal axes are the temporal period T^+ and the wavelength λ_x^+. In both controls, DR increases with increasing W_0^+. There exists the optimal time period of $T^+ \sim 100$ and wavelength of $\lambda_x^+ \sim 1000$ in temporally- and spatially-periodic controls, respectively. In general, the spatially-periodic control achieves higher DR than the temporally-periodic control. Figures 3 and 4 show comparison between two controls in terms of the gain G and the energy saving rate S. The spatially-periodic control gives higher G and S than the temporally-periodic control. From these results, we conclude that the spatially-periodic control is superior in terms of both the gain G and the energy saving rate S.

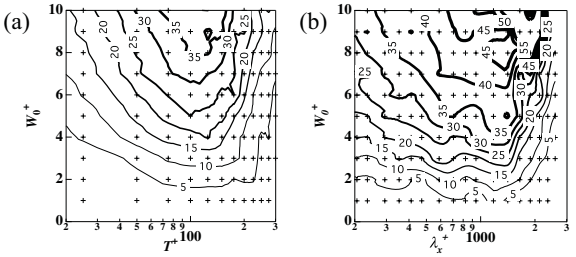

Fig. 2 $DR \times 100$ (%) as a function of time period, wavelength and amplitude: (a) temporally-periodic control, (b) spatially-periodic control.

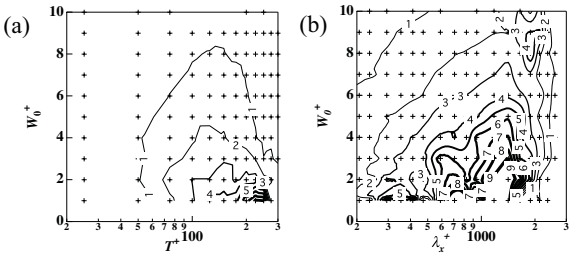

Fig. 3 G as a function of time period, wavelength and amplitude: (a) temporally-periodic control, (b) spatially-periodic control.

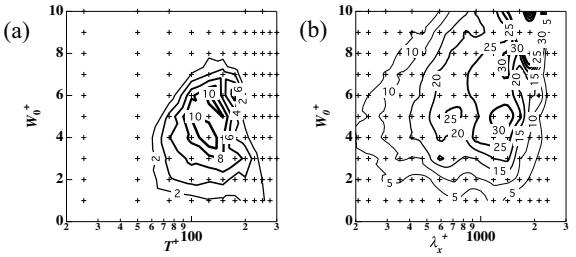

Fig. 4 $S \times 100$ (%) as a function of time period, wavelength and amplitude: (a) temporally-periodic control, (b) spatially-periodic control.

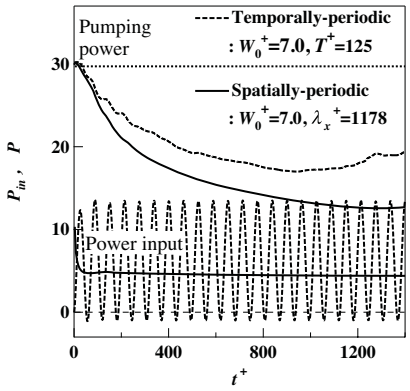

Fig. 5 Time traces of pumping power and control power input.

Figure 5 shows time traces of the pumping power input P_{in} in the temporally- and spatially-periodic controls when T^+ = 125 and λ_x^+ = 1178, respectively. The amplitude is fixed at W_0^+ = 7.0 in both cases. Comparing the two controls, the time-averaged power input is almost the same, while the friction drag is more reduced in the spatially-periodic control. This explains why a higher net energy saving rate is achieved in the spatially-periodic control as shown in Fig. 4.

To interpret the physical meaning of the optimum time period and wavelength in these controls, we assume a typical convection velocity of the coherent vortices as $u_c^+ \sim 10$ at $y^+ \sim 15$. Then, we can convert the spatial periodicity into the temporal periodicity as follows:

$$T_c^+ = \lambda_x^+ / u_c^+ . \tag{7}$$

If λ_x^+ = 1000, the equivalent temporal period of the spatially-periodic control is $T_c^+ \sim 100$, which agrees well with the optimum period of the temporally-periodic control. It is known that the dynamics of coherent structures have a periodical generation-destruction cycle (Jimenez and Moin, 1991; Kawahara and Kida, 2001). The present results suggest that the spanwise fluctuation of this particular frequency at the position of $y^+ \sim 15$ is effective in diminishing the coherent structures near the wall.

MECHANISMS OF DRAG REDUCTION

Phase Analysis

To explore the mechanisms of drag reduction in temporally- and spatially-periodic controls, we coordinated additional computations for each of the temporal period T^+ = 125 and the wavelength λ_x^+ = 1178. In both computations, the amplitude is set to be W_0^+ = 7.0. These are run under a constant pressure gradient in order to keep the wall shear stress constant excluding the Reynolds number effects.

When a periodic control is imposed, the resultant velocity field can be considered as a superposition of periodic and irregular fluctuations. Therefore, the instantaneous velocity u_i is decomposed into a spatio-temporal mean component $\overline{u}_i$, a phase fluctuation component $\tilde{u}_i$ and a random incoherent component u_i'':

$$u_i = \overline{u}_i + \tilde{u}_i + u_i''. \tag{8}$$

A phase-averaged quantity is given by:

$$\overline{u}_i + \tilde{u}_i = \langle u_i \rangle_\phi = \lim_{N\to\infty} \frac{1}{N} \sum_{n=0}^{N} u_i(\phi). \tag{9}$$

Figure 6 to 8 show the phase fluctuations of each velocity component. It is found that $\tilde{u}$ and $\tilde{v}$ are much smaller than that of $\tilde{w}$. It should be noted that $\tilde{v}$ in the temporally-periodic control is analytically zero due to the continuity equation. In addition, the temporal or spatial oscillation period of $\tilde{u}$ and $\tilde{v}$ is a half of that of $\tilde{w}$. This is due to the symmetric property of the present flow.

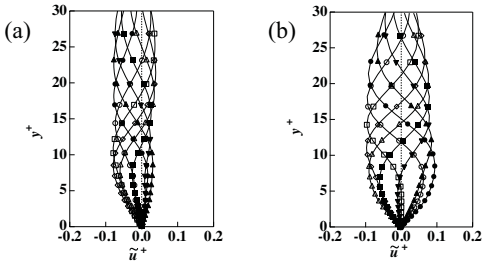

Fig. 6 Phase fluctuation parts of $\tilde{u}$. (a) temporally-periodic control, (b) spatially-periodic control.

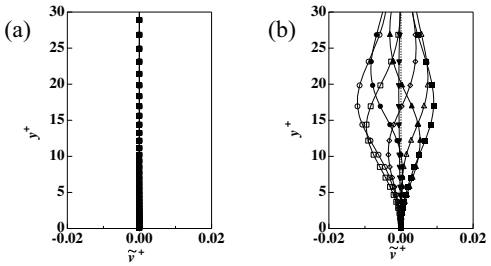

Fig. 7 Phase fluctuation parts of $\tilde{v}$. (a) temporally-periodic control, (b) spatially-periodic control.

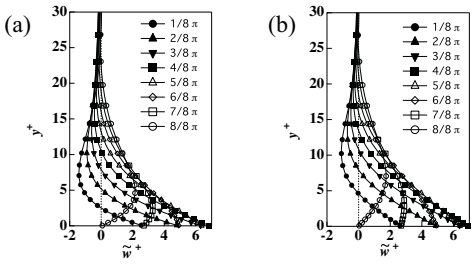

Fig. 8 Phase fluctuation parts of $\tilde{w}$. (a) temporally-periodic control, (b) spatially-periodic control.

Fukagata *et al*. (2001) shows that, for a fully developed channel flow, the friction drag coefficient C_f is represented as an integral equation with the Reynolds stress $-\overline{u'v'}$:

$$C_f = \frac{12}{\mathrm{Re}_b} + 12\int_{2\delta} (1-y)(-\overline{u'v'})dy. \tag{10}$$

Equation (10) is normalized by twice the bulk velocity $2U_b$ and the channel half-width δ. This equation means that the suppression of Reynolds stress near the wall is primarily

important. The Reynolds stress can be decomposed by Eq. (8) into two parts, i.e., the phase fluctuation component $-\tilde{\tilde{u}}\tilde{\tilde{v}}$, and the random component $-\overline{u''v''}$ as:

$$C_f = \frac{12}{\mathrm{Re}_b} + 12\int_{2\delta}(1-y)(-\tilde{\tilde{u}}\tilde{\tilde{v}} - \overline{u''v''})dy. \qquad (11)$$

Contributions of the above two Reynolds stresses are shown in Fig. 9. It is revealed that contribution of $-\tilde{\tilde{u}}\tilde{\tilde{v}}$ is negligibly small so that $-\overline{u''v''}$ governs the friction drag in both controls. In order to investigate the phase dependency of $-u''v''$, $-\widetilde{u''v''}$ at different phases are also plotted in Fig. 9. The phase change of $-\widetilde{u''v''}$ in the spatially-periodic control is larger than that in the temporally-periodic control. This is because the correlation between u'' and v'' is more sensitive to the phase in the spatially-periodic control as shown in Fig. 10.

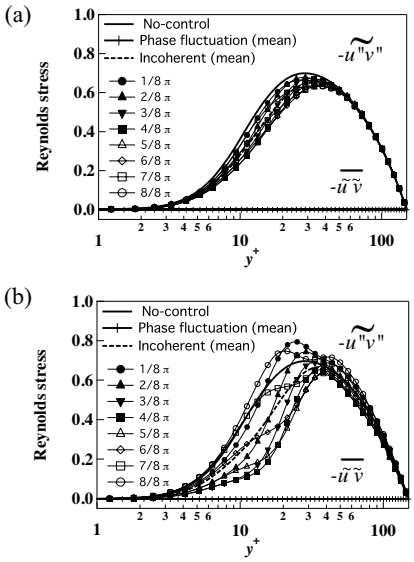

Fig. 9 Phase change of the Reynolds stresses, $-\tilde{\tilde{u}}\tilde{\tilde{v}}$ and $-u''v''$: (a) temporally-periodic control, (b) spatially-periodic control.

Quadrant Analysis

The incoherent Reynolds stress is further divided into four events depending on the signs of u'' and v''.

1. Q1 event; $u'' > 0$ and $v'' > 0$.
2. Q2 event; $u'' < 0$ and $v'' > 0$.
3. Q3 event; $u'' < 0$ and $v'' < 0$.
4. Q4 event; $u'' > 0$ and $v'' < 0$.

It is known that the above-mentioned four events are associated with a longitudinal vortex near the wall. According to Eq. (10), Q2 and Q4 events contribute to increase drag, while Q1 and Q3 decrease drag.

The contribution of each event is shown in Fig. 11. Vertical axis is the weighted Reynolds stress in Eq. (11). Although the contributions of four events decrease in both controls, Q2 and Q4 events are reduced most significantly. This suggests that the drastic decrease in Q2 and Q4 is a primary reason for drag reduction in both controls. In addition, Q2 event in the spatially-periodic control is more attenuated than that in the temporally-periodic control. This explains why the spatially-periodic control is more effective in reducing drag.

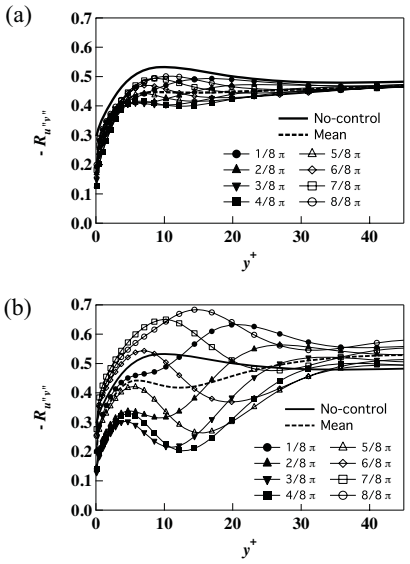

Fig. 10 Correlation between u'' and v'': (a) temporally-periodic control, (b) spatially-periodic control.

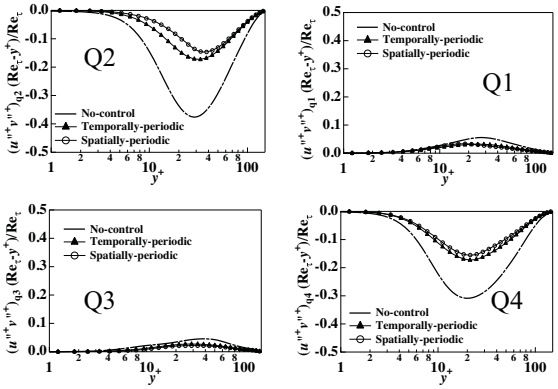

Fig. 11 Quadrant contribution of the incoherent Reynolds stress $-\overline{u''v''}$.

Conditional Sampling

In order to further explore the turbulent structure under control, we calculate the conditional average of the flow field around the longitudinal vortex near the wall. First, we capture a longitudinal vortex by searching the point where the second invariant Q^+ of deformation tensor is smaller than - 0.02 in the larger of y^+ = 10 - 20. Among these selected points, we define vortex cores (c_z, c_y), where the local pressure becomes minimum. Since the response of the longitudinal vortex to wall velocity should depend on its rotational direction, we only choose vortex cores with $\omega_x > 0$. Then, we average the velocity field around the core for $\Delta z^+ = z^+ - c_z = -40 \sim 40$ in the spanwise direction, and $y^+ = 0 \sim 40$ in the wall-normal direction.

Figure 12 shows the number of detected vortex cores. The horizontal axis is phase number n, which represents each phase of $n/8\pi$ during the period. The total number of

vortices is increased by 59% than that of uncontrolled in the temporally-periodic control, and decreased by 5.35% in the spatially-periodic control. Especially, the number of vortices at the phases of $2/8\pi \sim 7/8\pi$ is decreased in both controls, this trend is more prominent in the spatially-periodic control. If we detect negative vortex cores, the number of detected vortices is increased at $2/8\pi \sim 7/8\pi$ and decreased at $10/8\pi \sim 15/8\pi$. Then, it is assumed that the phase-dependency of $-u''v''$ is caused by the number of longitudinal vortices at each phase.

Figure 13 shows conditionally sampled flow structures. The spatial relationship of the low-speed streak and the longitudinal vortex is drastically changed at each phase. This trend agrees well with Choi *et al*. (2002) for spanwise wall-oscillation control. We consider these changes are the main reason for the reduction of $-u''v''$. At $1/8\pi \sim 7/8\pi$, the spanwise wall velocity is positive, so that it opposes to the vortex motion above the wall. As a result, the low-speed streak region disappears, so that Q2 event is reduced. At $10/8\pi \sim 16/8\pi$, the spanwise wall velocity becomes negative, and high-speed region is dragged into below the vortex. As the same time, the low-speed streak is pushed up above the vortex. Then, Q2 event migrates far from the wall, and Q4 event gets weak because the positive u'' becomes small. In summary, Q2 event is always reduced regardless of the direction of wall velocity and the number of vortices.

CONCLUSIONS

We investigated the effects of temporally- and spatially-periodic spanwise control input on the near-wall coherent structures and the resultant drag reduction. As a result, we draw the following conclusions:

1. Spatially-periodic control achieves better performance than temporally-periodic control. The spatially-periodic control can get larger drag reduction rate *DR* than temporally-periodic control at the same power input. The gain *G* and the energy saving rate *S* are generally larger in the spatially-periodic control than those in the temporally-periodic control.
2. In both temporally- and spatially-periodic controls, there exist the optimal values for the time period of $T^+ \sim 100$ and wavelength $\lambda_x^+ \sim 1000$ in terms of drag reduction. Taking into account the typical convection velocity of coherent structures near the wall, the above optimal wavelength $\lambda_x^+ \sim 1000$ coincides with the optimal time period. This suggests that the spanwise fluctuation of $T_c^+ \sim 100$ is effective in diminishing the active coherent structures near the wall.
3. By decomposing the Reynolds stress into phase-fluctuating and random components, it is found that the random component is dominant in both temporally- and spatially-periodic controls. The random component of the Reynolds stress tends to diminish when the wall velocity amplitude reaches its maximum value. In addition, this phase-dependency is more significant in the spatially-periodic control.
4. A conditionally-averaged flow field shows that the low-speed streak associated with the longitudinal vortex is drastically damped at the wall, regardless of the direction of wall velocity. They result in a decrease of Q2 and Q4 event near the wall and also frictional drag regardless of the number of the longitudinal vortices.

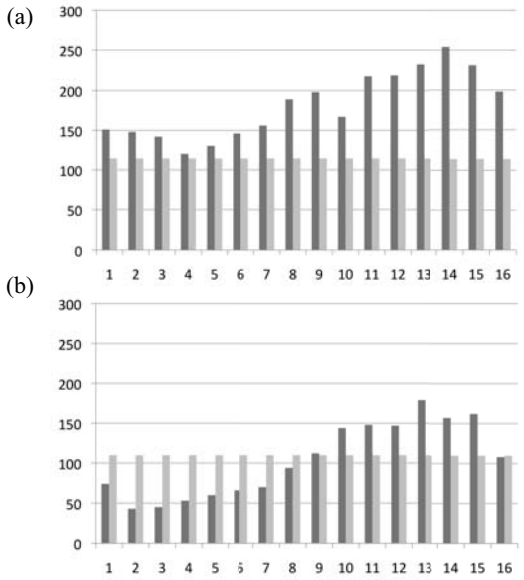

Fig. 12 The number of detected vortices; gray bar is uncontrolled, black bar is controlled: (a) temporally-periodic control, (b) spatially-periodic control.

ACKNOWLEDGMENTS

This work was financially supported through the Grant-in-Aid for Scientific Research (A) (No.20246036) by the Ministry of Education, Culture, Sports, Science and Technology (MEXT).

REFERENCES

Choi, J-. I., Xu, C-. X. and Sung, H. J., 2002, "Drag reduction by spanwise wall oscillation in wall-bounded turbulence flows," AIAA Journal, Vol. 40, No. 5, pp. 842-850.

Du, Y., and Karniadakis, G. E., 2000, "Suppressing wall-turbulence via a transverse traveling wave", Science, Vol. 288, pp. 1230-1234.

Filippone, A., 2000, "Data and performances of selected aircraft and rotorcraft", Progress in Aerospace Science, Vol. 36, pp. 629-654.

Fukagata, K., Iwamoto, K. and Kasagi, N., 2002, "Contribution of Reynolds stress distribution to the skin friction in wall-bounded flows," Phys. of Fluids, Vol. 14, L73-L76.

Jimenez, J. and Moin, P., 1991, "The minimal flow unit in near-wall turbulence," J. Fluid Mech., Vol. 225, pp. 213-240.

Jung, W., J., Mangiavacchi, N. and Akhavan, R., 1992, "Suppression of turbulence in wall-bounded floes by high frequency spanwise oscillations", Phys. Fluids A, Vol. 6, pp. 335-359.

Kawahara, G. and Kida, S, 2001, "Periodic motion embedded in plane Couette turbulence: regeneration cycle and burst," J. Fluid Mech., Vol. 449, pp. 291-300.

Quadrio, M., and Ricco, P., 2004, "Critical assessment of turbulent drag reduction through spanwise wall oscillations", J. Fluid Mech., Vol. 521, pp. 251-271.

Tardu, S., 1998, "Near wall turbulence control by local time periodical blowing," Experimental Thermal and Fluid Science, Vol. 16, pp. 41-53.

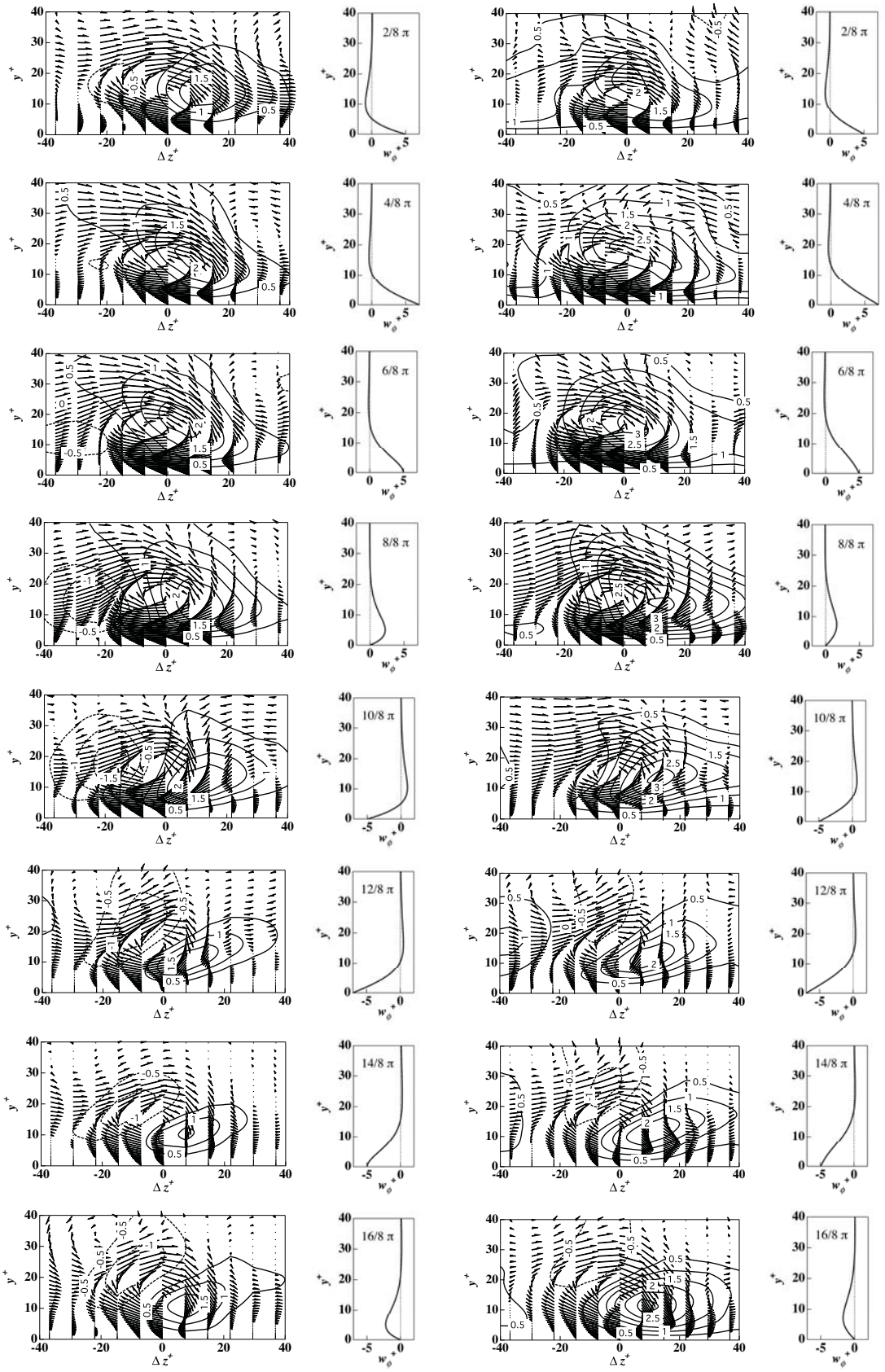

Fig. 13 Conditionally-sampled flow structures shown with *v" – w"* velocity vectors and *u"*- contours, when $\omega_x > 0$: left is temporally-periodic control, and right is spatially-periodic control.